Stem Cell Reports
Report
ISSCR
OPEN ACCESS

Human pluripotent stem cell-derived eosinophils reveal potent cytotoxicity against solid tumors

Weifeng Lai,[1,4] Huangfan Xie,[1,4] Yuting Liu,[2] Feng Zheng,[1] Yingfeng Zhang,[1] Qi Lei,[1] Lejun Lv,[1] Jiebin Dong,[1] Jian Song,[1] Xue Gao,[1] Ming Yin,[3] Chengyan Wang,[1,*] and Hongkui Deng[1,*]

[1]School of Basic Medical Sciences, State Key Laboratory of Natural and Biomimetic Drugs, Peking University Health Science Center, and the MOE Key Laboratory of Cell Proliferation and Differentiation, College of Life Sciences, Peking-Tsinghua Center for Life Sciences, Peking University, Beijing 100191, China

[2]Center for Bioinformatics, School of Life Sciences, Center for Statistical Science, Peking University, Beijing 100871, China

[3]Beijing Vitalstar Biotechnology, Beijing 100012, China

[4]These authors contributed equally

*Correspondence: chengyanw@pku.edu.cn (C.W.), hongkui_deng@pku.edu.cn (H.D.)

https://doi.org/10.1016/j.stemcr.2021.06.005

SUMMARY

Eosinophils are attractive innate immune cells to use to potentiate T cell antitumor efficacy because they are capable of infiltrating tumors at early stages and modulating the tumor microenvironment. However, the limited number of functional eosinophils caused by the scarcity and short life of primary eosinophils in peripheral blood has greatly impeded the development of eosinophil-based immunotherapy. In this study, we established an efficient chemically defined protocol to generate a large quantity of functional eosinophils from human pluripotent stem cells (hPSCs) with nearly 100% purity expressing eosinophil peroxidase. These hPSC-derived eosinophils transcriptionally resembled their primary counterpart. Moreover, hPSC-derived eosinophils showed competent tumor killing capacity in established solid tumors. Furthermore, the combination of hPSC-derived eosinophils with CAR-T cells exhibited potential synergistic effects, inhibiting tumor growth and enhancing mouse survival. Our study opens up new avenues for the development of eosinophil-based immunotherapies to treat cancer.

INTRODUCTION

Adaptive T cell therapy has made breakthroughs in hematologic malignancies (Guedan et al., 2019). However, it still remains challenging for solid tumor treatment because of the barrier that prevents T cells from infiltrating the tumor and the immunosuppressive microenvironment (Majzner and Mackall, 2019). Increasing studies have demonstrated that innate immune cells play crucial roles in inducing the T cell immunity response and regulating the tumor microenvironment, which makes them promising innate immune cells for potentiating T cell antitumor efficacy (Demaria et al., 2019).

Among the different innate immune cell types, eosinophils are attractive immune effector cells because of their potential for improving immunotherapies. Eosinophils possess the unique advantage of quickly infiltrating tumors in the early response (Carretero et al., 2015; Reichman et al., 2016). After infiltration of tumors, eosinophils express multiple chemokine and alarmin receptors that allow them to orchestrate antitumor immunity from the following different aspects: first, infiltrated eosinophils could enhance the infiltration of antigen-specific T cells into the tumors (Carretero et al., 2015); second, they can regulate the tumor microenvironment with antitumorigenic properties; and third, they can produce dendritic cell and T helper cell chemoattractants (Rosenberg et al., 2013). Aside from the above studies in the mouse model, an increasing number of clinical studies show that the high efficiency of eosinophil infiltration of tumors correlates with a better prognosis in certain solid tumors (Gebhardt et al., 2015; Prizment et al., 2016; Weide et al., 2016). Moreover, eosinophils display antitumorigenic activity *in vitro* that is mediated by secretory granules (Spencer et al., 2014). The above studies have demonstrated that eosinophils hold great promise as a new type of immunotherapeutic cell for cancer treatment.

To develop eosinophil-based immunotherapy, one prerequisite is to generate a large number of functional human eosinophils. However, eosinophils are present in rather low numbers in peripheral blood, representing less than 3% of the total population of leukocytes (Weller and Spencer, 2017), and their half-life is comparatively short, ranging from 18 h to several days (Rosenberg et al., 2013). To resolve the shortage problem of functional eosinophils, one promising strategy is to generate unlimited numbers of functional mature eosinophils from human pluripotent stem cells (hPSCs).

In this study, we describe a highly efficient, chemically defined approach designed for just this purpose, based on our previously developed protocol for generating hematopoietic progenitor cells (HPCs) (Wang et al., 2012). We further show that these cells are able to directly kill various human tumor cells both *in vitro* and *in vivo* and demonstrate potential synergistic efficacy in suppressing established tumors by combining with CAR-T cells. Therefore, these hPSC-derived eosinophils could prove to be critical for the development of new strategies to facilitate cancer immunotherapy.

RESULTS

Efficient differentiation of eosinophils from human embryonic stem cells

The present protocol to generate eosinophils from human embryonic stem cells (hESCs) (H1) is modified from our previous study that produced HPCs from hPSCs (Wang et al., 2012). In our present method, we generated eosinophils in the order mesodermal progenitors, hemogenic endothelial cells, and HPCs using the specified differentiation media (Figure 1A).

We first monitored the generation of eosinophils from HPCs. $CD34^+CD45^+$ HPCs were generated and expanded from differentiation day 12 (E0) to differentiation day 16 (E4). These cells then gradually lost the expression of CD34 and became nearly completely $CD34^-CD45^+$ hematopoietic cells on E20 (Figure S1A). In the meantime, we traced the expression of the eosinophil-specific marker eosinophil peroxidase (EPX), which showed the earliest production of EPX^+ cells on E4 (Figures 1B and 1C). On E20, 98% of cells in the final culture of differentiation were EPX^+ cells (Figures 1B and 1C). Consistent with this, we found that the percentage of SSC^{high} cells gradually increased from 21.5% to 94.3% between E0 and E20, indicating a maturation of eosinophils with increasing level of cellular complexity (Figure S1B). We further analyzed the mature eosinophils and found that these cells expressed the active and mature eosinophil markers (Figure 1D). In addition, we further confirmed the expression of eosinophil-specific genes with immunostaining (Figures S1C and S1D). In parallel, basophil-specific genes could not be detected from E0 to E20 by immunostaining or RNA sequencing (RNA-seq) (Figures S1D and S1E). We next performed Giemsa staining and electron microscopy to further characterize these EPX^+ cells. These cells displayed the typical features of eosinophils, possessing bilobed nuclei and abundant granules in the cytoplasm (Figure 1E). The granules of these cells were highly electron dense, consistent with the characteristics of granular proteins (Figure 1F). Eosinophils were generated at approximately 1,000-fold, that is, nearly 1,000 eosinophils were generated from a single initiating hESC (Figure 1G). Taken together, these results indicated that we successfully established a protocol that robustly generated eosinophils from hESCs with a high level of purity.

Transcriptional analysis of hESC-derived eosinophils

We next investigated the transcriptional fidelity of the eosinophil differentiation by conducting RNA-seq studies. Hierarchical clustering revealed that hESC-derived eosinophils (E20) clustered closely with primary naive eosinophils, and the differentiation process involved a PSC-to-eosinophil transition with a stage-specific clustering pattern (Figures 2A and 2B). Key eosinophil developmental regulators, such as the transcription factors *CEBPA*, *CEBPE*, *SPI1*, and *GATA1* (Reichman et al., 2016) and the receptors *IL5RA*, *CSF2RB*, *ADGRE1*, and *CD52* (Davis and Rothenberg, 2014), showed a gradual increase in expression from H1 to D32 (E20) eosinophils. Notably, the expression of the maturation marker *Siglec-8* (Rosenberg et al., 2013) was induced only at the later stages (Figure 2B). Compared with H1 cells, D32 (E20) eosinophils possessed high levels of the granular proteins *EPX*, *RNASE2*, *RNASE3*, *PRG2*, and *PRG3*, which are known to play pivotal roles in eosinophil cytotoxicity (Acharya and Ackerman, 2014) (Figure 2B). hPSC-derived eosinophils exhibited high expression levels of *IL5RA*, *CD244*, and *ITGB2* (*CD11b*) in the later stages (Figure 2B), of which CD244 can enhance antitumor effects by mediating eosinophil and natural killer cell degranulation (Lee et al., 2006). Impressively, the above genes were expressed in E20 hESC-derived cells at a level comparable to that seen in cord-blood-derived naive eosinophils.

To further confirm eosinophil-specific gene expression in the differentiated cells, we performed real-time qPCR on the induced cells on days 0 (H1), 12 (E0), 28 (E16), and 32 (E20) and on primary naive eosinophils (CB-E), and found that they exhibited high expression levels of *EPX*, *PRG2*, *PRG3*, *RNASE2*, *RNASE3*, and *IL5RA* in the later stages, comparable to primary naive eosinophils (Figure 2C).

We next performed Gene Ontology (GO) term and KEGG pathway analyses on the RNA-seq data. The most upregulated GO terms and pathways in day 32 (E20) eosinophils are shown in Figure 2D. As the results show, several pathways that are characteristic of innate immune responses were highly expressed in our induced eosinophils. In addition, these cells were highly associated with the terms "lysosome" and "lysosomal membrane," both of which are features of cells with large numbers of excretory granules. Taken together, the gene expression profiling strongly suggests a conversion of hESCs to fully competent eosinophils.

Functional assessment of the *in vitro* tumoricidal activity of hESC-derived eosinophils

We next assessed the tumoricidal properties of the hESC-derived eosinophils against three tumor cell lines: HCT116 (human colorectal carcinoma), MDA-MB-231 (human breast adenocarcinoma), and HepG2 (human hepatocellular carcinoma).

The H1-derived eosinophils exerted significant tumoricidal activity toward these tumor cells. Our data showed that H1-derived eosinophils showed competence in lysis ability of 40%–60% at 1:1 effector-to-target ratio, which was comparable to that of naive

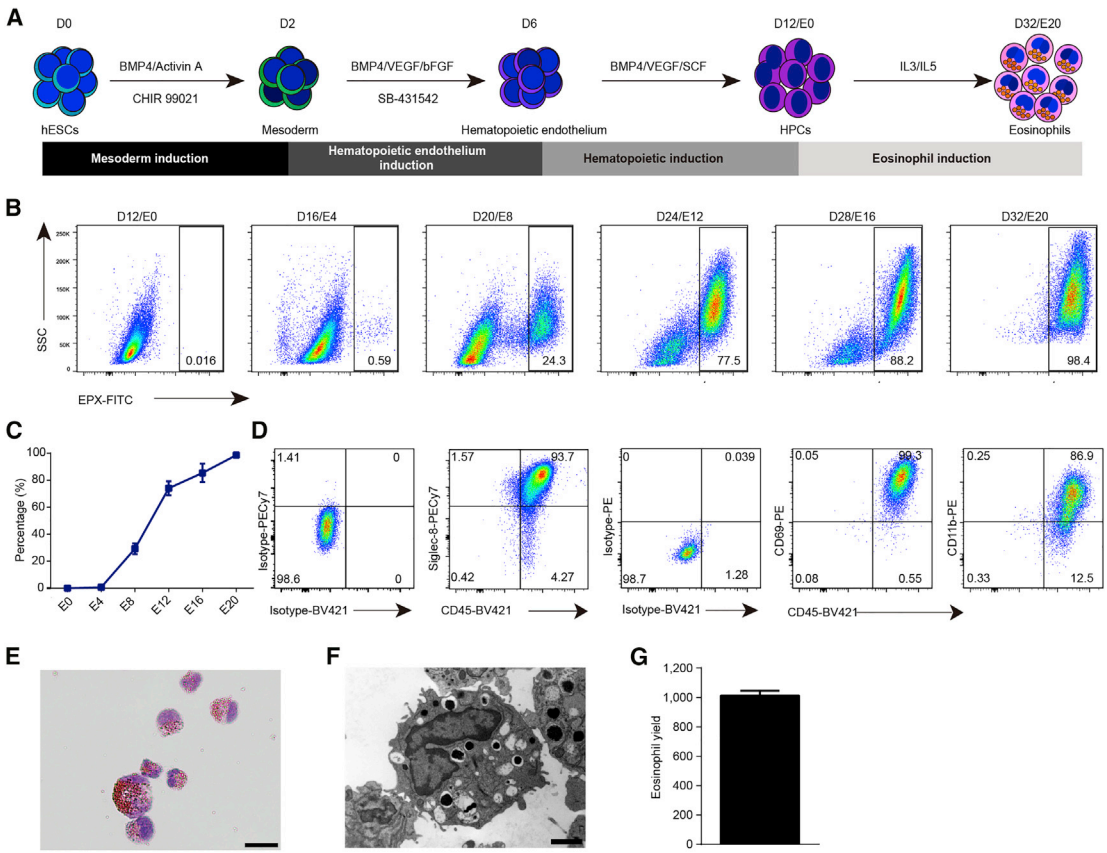

Figure 1. Efficient generation of eosinophils from hESCs

(A) Experimental schematic for the differentiation of hESCs into eosinophils.

(B) Representative flow plots from four independent experiments showing the generation of EPX^+ cells during eosinophil induction from E0 to E20.

(C) Percentage of EPX^+ cell population during the eosinophil induction process from starting H1 cells (n = 4 independent experiments). Data shown as the mean value ± SD.

(D) Representative flow plots from three independent experiments showing staining for the indicated surface marker on H1-derived eosinophils recovered on E20.

(E) Giemsa staining of induced cells recovered on E20. Scale bar, 20 μm.

(F) Electron microscope image of induced cells recovered on E16. Scale bar, 2 μm.

(G) Representative eosinophil yield at E16 from one H1 initiated cell (n = 3 independent experiments). Data shown as mean value ± SD. See also Figure S1.

eosinophils (Figures 3A–3C). However, we did not observe the cytotoxicity of hPSC-derived eosinophils on human mesenchymal stem cells, human embryonic fibroblasts, or human umbilical vascular and endothelial cells (Figure S2A). These data demonstrate that hESC-derived eosinophils possessed highly specific cytotoxicity against tumor cells *in vitro*.

Functional assessment of the *in vivo* tumoricidal activity of hESC-derived eosinophils

To determine whether our hESC-derived eosinophils were capable of infiltrating tumors, we first injected H1-derived eosinophils into immunodeficient NPG mouse recipients that were preconditioned with human tumors formed by HCT116 cells by subcutaneous transplantation, and then analyzed the tumors at 48 h after eosinophil injection. Immunohistochemistry revealed that hESC-derived eosinophils (EPX^+ cells) infiltrated tumors (Figures S2B–S2D). By using flow cytometry analysis, we detected an apparent human $CD45^+$ cell population inside the tumors (Figure S2E), indicating that hESC-derived eosinophils are able to infiltrate tumors. Further, we tested the infiltration of hPSC-derived eosinophils in main organs and tissues, and the data showed a few hPSC-derived eosinophils detected in the spleen, but not in brain, heart, liver, lung, kidney, intestine, or colon (Figure S2F).

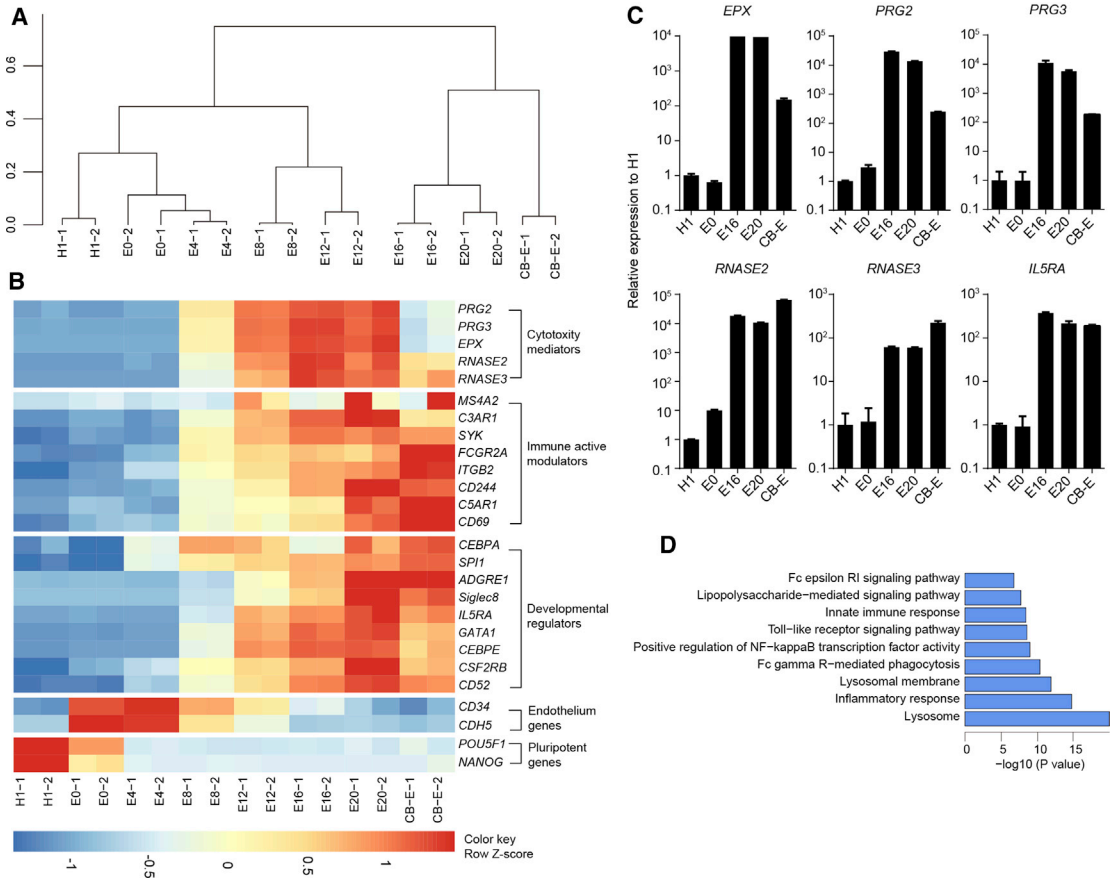

Figure 2. Transcriptional analysis of H1-derived eosinophils

(A) Dendritic hierarchical clustering of global gene expression of H1 cells and induced cells harvested on E0, E4, E8, E12, E16, and E20. Cord-blood-derived naive eosinophils (CB-E) were used as a positive control. Notably, the cells on E0 were sorted for $CD34^+$ cell population for transcriptional analysis, while the whole cell culture was collected for transcriptional analysis on E4, E8, E12, E16, and E20. For cells at each time point, duplicate experiments were performed.

(B) Heatmaps of indicated gene expression, including cytotoxicity mediators, immune active modulators, developmental regulators, endothelium genes, and pluripotency genes in H1, CB-E, and induced cells harvested on E0, E4, E8, E12, E16, E20, and CB-E based on *Z* score from FPKM.

(C) Real-time qPCR analysis of key eosinophil gene expression in cells recovered on D0, E0, E16, and E20. Cord-blood-derived naive eosinophils (CB-E) were used as a positive control (n = 2). Data are shown as mean value ± SD. Similar results were obtained in three independent experiments.

(D) GO term and KEGG analysis showing GO terms and KEGG pathways that were upregulated in H1-derived eosinophils collected on E20 compared with H1.

We next investigated the *in vivo* antitumor activity of the hESC-derived eosinophils. We first inoculated tumor cells (HCT116) into immunodeficient NPG mouse recipients to establish tumor-xenograft models. Then we injected H1-derived eosinophils into the tumor-bearing mice (Figure 3D). As the bioluminescence imaging showed, the injection of eosinophils significantly inhibited tumor growth in HCT116-tumor-bearing mice (Figure 3E). The eosinophil infusion evidently prolonged the median survival time of the HCT116-tumor-bearing mice compared with the untreated group (Figure 3F). In addition, the infusion of eosinophils significantly suppressed tumor growth (Figure S2G) and prolonged the median survival time of MDA-MB-231-tumor-bearing mice (Figure S2H). Taken together, these results demonstrate that hESC-derived eosinophils possess tumoricidal properties *in vivo*.

Next, we evaluated the tumoricidal efficacy of hESC-derived eosinophils in established tumors. HepG2 cells were injected into each mouse and 60–70 mm^3 tumors were established on day 7 (Figures 4A and S2I). hESC-derived eosinophils were injected into tumor-bearing mice at the 7- and 10-day timepoints (Figure 4A). We found

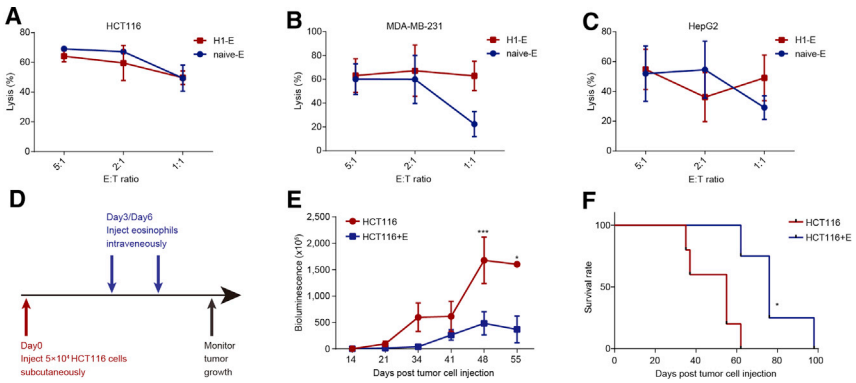

Figure 3. Potent cytotoxicity of hESC-derived eosinophils against solid tumors *in vitro* and *in vivo*

(A–C) Cytotoxicity of the H1-derived eosinophils (H1-E) and cord-blood-derived eosinophils (naive-E) toward HCT116 (A), MDA-MB-231 (B), and HepG2 (C) target cells at the indicated effector-to-target ratios (n = 3). The lysis rate of target cells is shown as the mean percentage value ± SD. n = 3 independent experiments.

(D) Schematic depicting the *in vivo* tumor assay.

(E) The HCT116 tumor cell burden of each group measured on the indicated days after tumor cell injection, as shown by bioluminescence imaging (n = 5 for control group; n = 4 for HCT116+E group). Statistical significance was assessed using two-tailed ANOVA, where *p < 0.05 and ***p < 0.001; data shown as mean values ± SEM.

(F) Kaplan-Meier curve representing the percentage survival of the experimental groups in the HCT116-xenograft mouse models (n = 5 for control group; n = 4 for HCT116+E group). Statistical analyses were calculated using log-rank (Mantel-Cox) test, where *p < 0.05.

See also Figure S2.

that the injection of hESC-derived eosinophils significantly inhibited the tumor growth (Figures 4B and 4C). Similarly, hESC-derived eosinophils also exhibited significant tumor inhibition effects on HCT116 colorectal carcinoma (Figure S2J). We further detected the safety of hPSC-derived eosinophils in main organs or tissues by hematoxylin and eosin staining after injecting different doses of hPSC-derived eosinophils. No abnormal morphology was observed at the doses we tested (Figure S3A). Taken together, these data demonstrate that hESC-derived eosinophils possess competent cytotoxic effects suppressing tumor growth in established solid tumors.

hESC-derived eosinophils enhanced tumor killing capacity of CAR-T cells *in vivo*

CAR-T cells may lose their antitumor effects against solid tumors due to inactivation of CAR-T cells induced by the immune-suppressive microenvironment (Newick et al., 2017). We next studied whether hESC-derived eosinophils could facilitate CAR-T cell antitumor efficiency in established solid tumors. We generated CAR-T cells through transduction of the HER2 CAR gene into peripheral blood T cells (Figures S3B and S3C). Then, we injected the cells into the established tumor-bearing mice divided into three experimental groups: CAR-T cells alone, hESC-derived eosinophils alone, and the combination of hESC-derived eosinophils and CAR-T cells (Figure 4D). The results showed that all three experiment groups significantly inhibited tumor growth in HCT116 tumor-bearing mice compared with the control group (Figure 4E). These three experiment groups apparently extended the survival time of the HCT116-tumor-bearing mice compared with the control group (Figure 4F). In particular, we found that the combination of CAR-T cells and hESC-derived eosinophils exhibited better antitumor effects against established tumors than CAR-T cells alone or hESC-derived eosinophils alone (Figures 4E, 4F, and S3D). Taken together, these results indicate a potential synergy of action when both eosinophils and CAR-T cells are used together.

Efficient differentiation of functional eosinophils from human iPSCs

We also generated EPX$^+$ eosinophils from human induced pluripotent stem cells (iPSCs) (Figure S4A and S4E). Real-time qPCR showed that the induced cells at E20 displayed upregulation of eosinophil-specific genes compared with iPSCs (Figures S4B and S4F). Human iPSC-derived eosinophils also exhibited potent tumor killing capacity on HepG2 and HCT116 cells *in vitro* (Figures S4C and S4G) and significantly suppressed tumor growth *in vivo* (Figures S4D and S4H). All these data demonstrate that functional mature eosinophils that possess competent cytotoxic effects on solid tumors can be derived from independent human iPSCs.

DISCUSSION

Here, we report the successful development of a protocol to efficiently generate large numbers of eosinophils expressing eosinophil-specific granule proteins and genes from hPSCs. We also demonstrate that these hPSC-derived eosinophils possess a high degree of cytotoxicity against diverse tumor cells in both *in vitro* and *in vivo* settings. In particular, we found that the combination of hPSC-derived eosinophils with CAR-T cells presents higher efficiency of tumor killing *in vitro* and inhibits tumor growth more effectively *in vivo*.

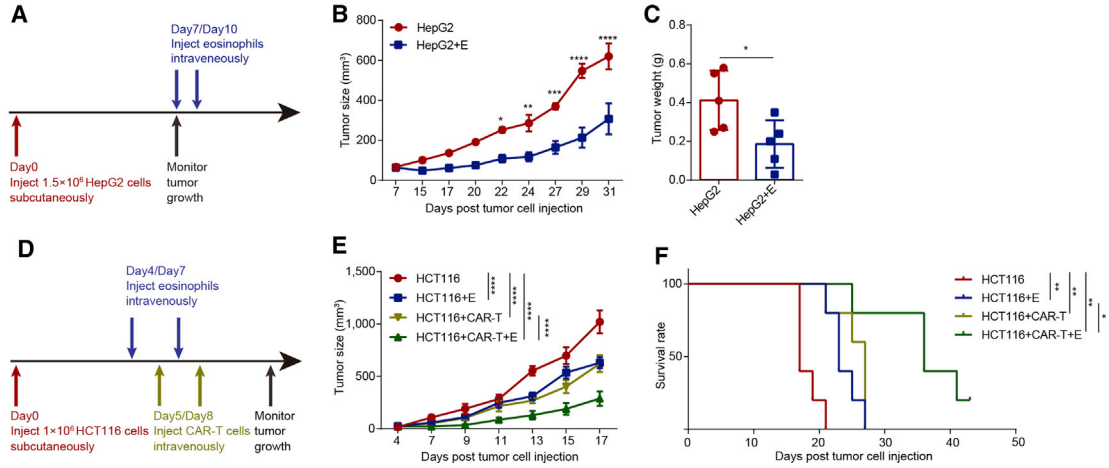

Figure 4. Enhanced tumoricidal activity of CAR-T cells against solid tumors by combination with hESC-derived eosinophils

(A) Schematic showing the *in vivo* tumor assay.

(B) HepG2 tumor size of each group was determined on the indicated days after tumor cell injection (n = 5 for each group). Statistical significance was assessed using two-tailed ANOVA, where *p < 0.05, **p < 0.01, ***p < 0.001, and ****p < 0.0001; data are shown as the mean values ± SEM.

(C) Tumor weight of HepG2 on day 32 (n = 5 for each group). Statistical significance was assessed using unpaired t test, where *p < 0.05, data are shown as the mean values ± SD.

(D) Schematic showing the *in vivo* tumor assay of CAR-T cells and hPSC-derived eosinophils.

(E) HCT116 tumor size of each group was measured on the indicated days after tumor cell injection (n = 5 for control group, CAR-T cell group, and combination group; n = 4 for hESC-derived eosinophil group). Statistical significance was assessed using two-tailed ANOVA compared with the HCT116 group, where ****p < 0.0001; data are shown as mean values ± SEM. These are representative data from two independent experiments.

(F) Kaplan-Meier curve representing the percentage survival of the experimental groups in the HCT116-xenograft mouse models (n = 5 for control group, CAR-T cell group, and combination group; n = 4 for hESC-derived eosinophil group). Statistical analyses were calculated using log-rank (Mantel-Cox) test, where*p < 0.05 and **p < 0.01. These are representative data from two independent experiments.

See also Figures S3 and S4.

Notably, hPSC-derived eosinophils produced in our study displayed eosinophil-specific features comparable to those of naive eosinophils. In terms of morphological phenotype, they exhibited bilobed nuclei, acidophilic stain incorporation, and electron-dense granules. At the transcriptional level, they expressed receptors involved in eosinophil survival and signal transduction, such as *IL5RA* and *Siglec-8* (Rosenberg et al., 2013) at high levels. In addition, these eosinophils also expressed cytotoxic granular proteins such as *EPX*, *PRG2*, *PRG3*, *RNASE2*, and *RNASE3*, which are known to be critical for the function of eosinophils with tumoricidal properties (Acharya and Ackerman, 2014). Most importantly, hPSC-derived eosinophils exhibited strong tumor killing activity, characteristic of naive eosinophils. Eosinophils lack surface T cell receptors and so should not cause graft-versus-host disease. With the advantage of hPSCs' ability to be genetically manipulated to establish HLA-deficient universal stem cells (Deuse et al., 2019), hPSC-derived eosinophils hold great potential as a universal, "off-the-shelf" cell source for immunotherapy.

Another advantage of our study is the development of a chemically defined approach to generate large quantities of functional human eosinophils from hPSCs. Although previous studies showed that hPSC-derived myeloid progenitors could generate MBP^+ eosinophils (Choi et al., 2009), these studies relied on stromal cells and serum, as well as the purification of hematopoietic progenitors. More importantly, EPX^+ eosinophils could be generated at a high purity and in large quantities, with nearly 1,000-fold increase from starting cells in number. Therefore, this protocol possesses multiple advantages that make it more suitable for future clinical applications.

Our study is the first report to demonstrate competent *in vivo* antitumor activity of hPSC-derived eosinophils and showed potential to facilitate CAR-T cell effects against solid tumors. According to the *in vivo* data for evaluating antitumor activity, hPSC-derived eosinophils exhibited strong efficacy, not only in inoculated tumors, but also in established tumors. Compared with other immune cell types, the major advantages of eosinophils' application in immunotherapy would be their capacity to respond at an

early stage and quickly infiltrate tumors, which could facilitate the attraction of T cells and regulate the tumor microenvironment to potentiate the T cell antitumor activity (Carretero et al., 2015). Our data showed that the combination of hPSC-derived eosinophils and CAR-T cells significantly inhibited tumor growth *in vivo*. This potential synergistic efficacy may result from the eosinophils' unique advantage of quick infiltration of tumors at the early response based on their expression of multiple chemokine and alarmin receptors (Carretero et al., 2015; Reichman et al., 2016). Their early infiltration of the tumor allowed the regulation of the tumor microenvironment with antitumorigenic properties or produced dendritic cell and T helper cell chemoattractants (Rosenberg et al., 2013). The eosinophils could directly lyse tumor cells, resulting in enhanced alarmin signals or chemokine secretion to enhance the infiltration of antigen-specific T cells into the tumors (Carretero et al., 2015). These features may potentiate the enhanced synergistic antitumor efficacy exhibited by CAR-T cells, and the underlying mechanisms are worth further study.

In summary, our study provides a robust method for generating unlimited numbers of functional human eosinophils for enhancing T cell antitumor activity, and this could represent an important step toward developing novel strategies of combining CAR-T cells with other immune cells for cancer immunotherapy.

EXPERIMENTAL PROCEDURES

Eosinophil differentiation from hESCs and iPSCs

hESCs (H1) and iPS cells (iPS-#7, iPS-#8) were cultured in Matrigel-coated plates at low density. Activin A, BMP4, and CHIR99021 were used to induce mesoderm. BMP4, VEGF, bFGF, and SB-431542 were used to induce hemogenic endothelial cells. BMP4, VEGF, SCF, NAC, and minocycline hydrochloride were used to induce HPCs. IL-3 and IL-5 were used to induce eosinophils. A detailed description is provided in the supplemental experimental procedures.

In vitro cytotoxicity assays

Tumor cells were seeded in 96-well plates. Six to ten hours later, the eosinophils were added to the target cells. After incubation for 20 h, the apoptotic cells of the tumor target cells were quantified by a standard bioluminescence assay. A detailed description is provided in the supplemental experimental procedures.

In vivo tumor assay

Luciferase-marked target cells were injected subcutaneously into recipient NPG mice, followed by two intravenous injections of E16–E20 hPSC-derived eosinophils. For established tumors, tumor cells were injected subcutaneously and eosinophils were injected intravenously. For evaluating the combination effects of CAR-T and hESC-derived eosinophils, tumor cells were injected subcutaneously. Two intravenous injections of eosinophils, CAR-T cells, or their combination were performed. A detailed description is provided in the supplemental experimental procedures.

Statistical analysis

Statistical analysis was performed with GraphPad Prism software. Data are shown as the means with standard deviation or means with standard error of the mean. Comparisons between groups were assessed using unpaired t test or two-tailed ANOVA as indicated. For all analyses, $p < 0.05$ was considered statistically significant. The statistical significance and n values are described in the figure legends. All the flow analysis data were processed with FlowJo v.10 software.

Data and code availability

RNA-seq data of this study have been deposited in the GEO database under accession no. GSE148907.

SUPPLEMENTAL INFORMATION

Supplemental information can be found online at https://doi.org/10.1016/j.stemcr.2021.06.005.

AUTHOR CONTRIBUTIONS

H.D. and W.L. conceived and designed the experiments. W.L., H.X., C.W., Y.L., F.Z., J.S., Y.Z., X.G., J.L., Q.L., J.D., and M.Y. performed experiments. H.D., H.X., and C.W. wrote the manuscript.

DECLARATION OF INTERESTS

H.D., C.W., W.L., and H.X. have filed a patent related to this work.

ACKNOWLEDGMENTS

We thank Professor Kuan-hui Xiang and Feng-ming Lu for gifting us the HepG2 cell line. We thank Jun Xu, Shi-cheng Sun, and Liew Soon Yi for assistance with the written paper. We thank Dr. Ying-Chun Hu, Yun-Chao Xie, and Peng-yuan Dong for their professional technical assistance in EM sample preparation and image analysis at the Core Facilities of the School of Life Sciences, Peking University. We thank the Flow Cytometry Core at the National Center for Protein Sciences at Peking University, particularly Hong-xia Lv, Li-ying Du, Huan Yang, and Yinghua Guo, for their technical help. This work was supported by the National Key Research and Development Program of China (2017YFA0103000), the National Natural Science Foundation of China (31730059, 31521004), and the Beijing Science and Technology Major Project (Z191100001519001).

Received: December 21, 2020
Revised: June 2, 2021
Accepted: June 4, 2021
Published: July 1, 2021

REFERENCES

Acharya, K.R., and Ackerman, S.J. (2014). Eosinophil granule proteins: form and function. J. Biol. Chem. *289*, 17406–17415.

Carretero, R., Sektioglu, I.M., Garbi, N., Salgado, O.C., Beckhove, P., and Hammerling, G.J. (2015). Eosinophils orchestrate cancer rejection by normalizing tumor vessels and enhancing infiltration of CD8(+) T cells. Nat. Immunol. *16*, 609–617.

Choi, K.D., Vodyanik, M.A., and Slukvin, I.I. (2009). Generation of mature human myelomonocytic cells through expansion and differentiation of pluripotent stem cell-derived lin-CD34+CD43+CD45+ progenitors. J. Clin. Invest. *119*, 2818–2829.

Davis, B.P., and Rothenberg, M.E. (2014). Eosinophils and cancer. Cancer Immunol. Res. *2*, 1–8.

Demaria, O., Cornen, S., Daeron, M., Morel, Y., Medzhitov, R., and Vivier, E. (2019). Harnessing innate immunity in cancer therapy. Nature *574*, 45–56.

Deuse, T., Hu, X., Gravina, A., Wang, D., Tediashvili, G., De, C., Thayer, W.O., Wahl, A., Garcia, J.V., Reichenspurner, H., et al. (2019). Hypoimmunogenic derivatives of induced pluripotent stem cells evade immune rejection in fully immunocompetent allogeneic recipients. Nat. Biotechnol. *37*, 252–258.

Gebhardt, C., Sevko, A., Jiang, H., Lichtenberger, R., Reith, M., Tarnanidis, K., Holland-Letz, T., Umansky, L., Beckhove, P., Sucker, A., et al. (2015). Myeloid cells and related chronic inflammatory factors as novel predictive markers in melanoma treatment with ipilimumab. Clin. Cancer Res. *21*, 5453–5459.

Guedan, S., Ruella, M., and June, C.H. (2019). Emerging cellular therapies for cancer. Annu. Rev. Immunol. *37*, 145–171.

Lee, K.M., Forman, J.P., McNerney, M.E., Stepp, S., Kuppireddi, S., Guzior, D., Latchman, Y.E., Sayegh, M.H., Yagita, H., Park, C.K., et al. (2006). Requirement of homotypic NK-cell interactions through 2B4(CD244)/CD48 in the generation of NK effector functions. Blood *107*, 3181–3188.

Majzner, R.G., and Mackall, C.L. (2019). Clinical lessons learned from the first leg of the CAR T cell journey. Nat. Med. *25*, 1341–1355.

Newick, K., O'Brien, S., Moon, E., and Albelda, S.M. (2017). CAR T cell therapy for solid tumors. Annu. Rev. Med. *68*, 139–152.

Prizment, A.E., Vierkant, R.A., Smyrk, T.C., Tillmans, L.S., Lee, J.J., Sriramarao, P., Nelson, H.H., Lynch, C.F., Thibodeau, S.N., Church, T.R., et al. (2016). Tumor eosinophil infiltration and improved survival of colorectal cancer patients: Iowa Women's Health Study. Mod. Pathol. *29*, 516–527.

Reichman, H., Karo-Atar, D., and Munitz, A. (2016). Emerging roles for eosinophils in the tumor microenvironment. Trends Cancer *2*, 664–675.

Rosenberg, H.F., Dyer, K.D., and Foster, P.S. (2013). Eosinophils: changing perspectives in health and disease. Nat. Rev. Immunol. *13*, 9–22.

Spencer, L.A., Bonjour, K., Melo, R.C., and Weller, P.F. (2014). Eosinophil secretion of granule-derived cytokines. Front. Immunol. *5*, 496.

Wang, C., Tang, X., Sun, X., Miao, Z., Lv, Y., Yang, Y., Zhang, H., Zhang, P., Liu, Y., Du, L., et al. (2012). TGFbeta inhibition enhances the generation of hematopoietic progenitors from human ES cell-derived hemogenic endothelial cells using a stepwise strategy. Cell Res. *22*, 194–207.

Weide, B., Martens, A., Hassel, J.C., Berking, C., Postow, M.A., Bisschop, K., Simeone, E., Mangana, J., Schilling, B., Di Giacomo, A.M., et al. (2016). Baseline biomarkers for outcome of melanoma patients treated with pembrolizumab. Clin. Cancer Res. *22*, 5487–5496.

Weller, P.F., and Spencer, L.A. (2017). Functions of tissue-resident eosinophils. Nat. Rev. Immunol. *17*, 746–760.

Stem Cell Reports, Volume *16*

Supplemental Information

Human pluripotent stem cell-derived eosinophils reveal potent cytotoxicity against solid tumors

Weifeng Lai, Huangfan Xie, Yuting Liu, Feng Zheng, Yingfeng Zhang, Qi Lei, Lejun Lv, Jiebin Dong, Jian Song, Xue Gao, Ming Yin, Chengyan Wang, and Hongkui Deng

Supplemental Information

Inventory of Supplemental Information

Supplemental Table and Figures

Supplemental Experimental Procedures

Figure S1

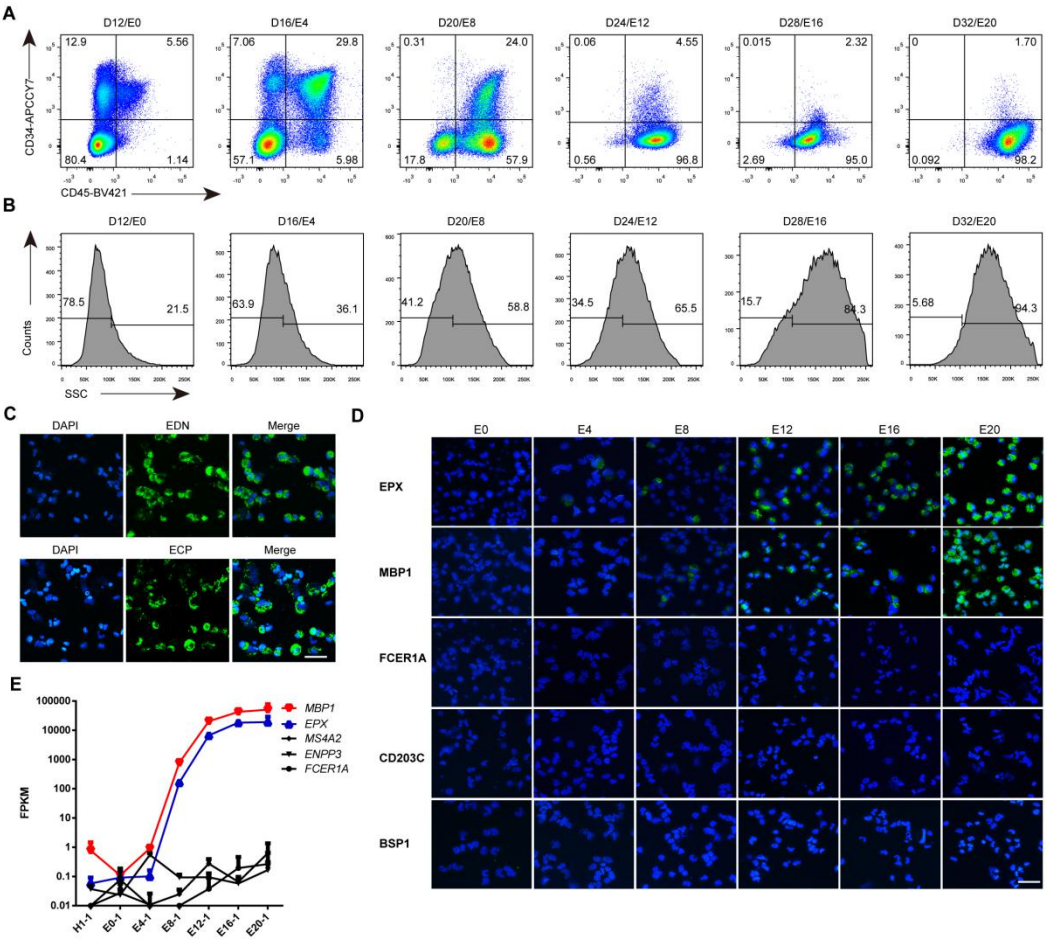

Figure S1. Generation of eosinophils from hESCs, related to Figure 1.

(A) Representative flow plots from 3 independent experiments showing the kinetics of the percentage of $CD34^{+}CD45^{+}$ cells during eosinophil induction from hESCs (H1).

(B) Representative flow histogram from 3 independent experiments showing the kinetics of the percentage of the SSC^{high} cells in the population during eosinophil induction from hESCs (H1).

(C) Representative immunostaining data from 3 independent experiments showing the EDN and ECP expression of E20 eosinophil induced from hESCs (H1), scale bar, 50 μm.

(D) Representative immunostaining data from 3 independent experiments showing the gene expression of induced cells harvested on E0, E4, E8, E12, E16 and E20, scale bar, 50 μm.

(E) Gene expression of H1 cells and induced cells harvested on E0, E4, E8, E12, E16 and E20 from RNA-seq data (n=2 replicate).

Figure S2

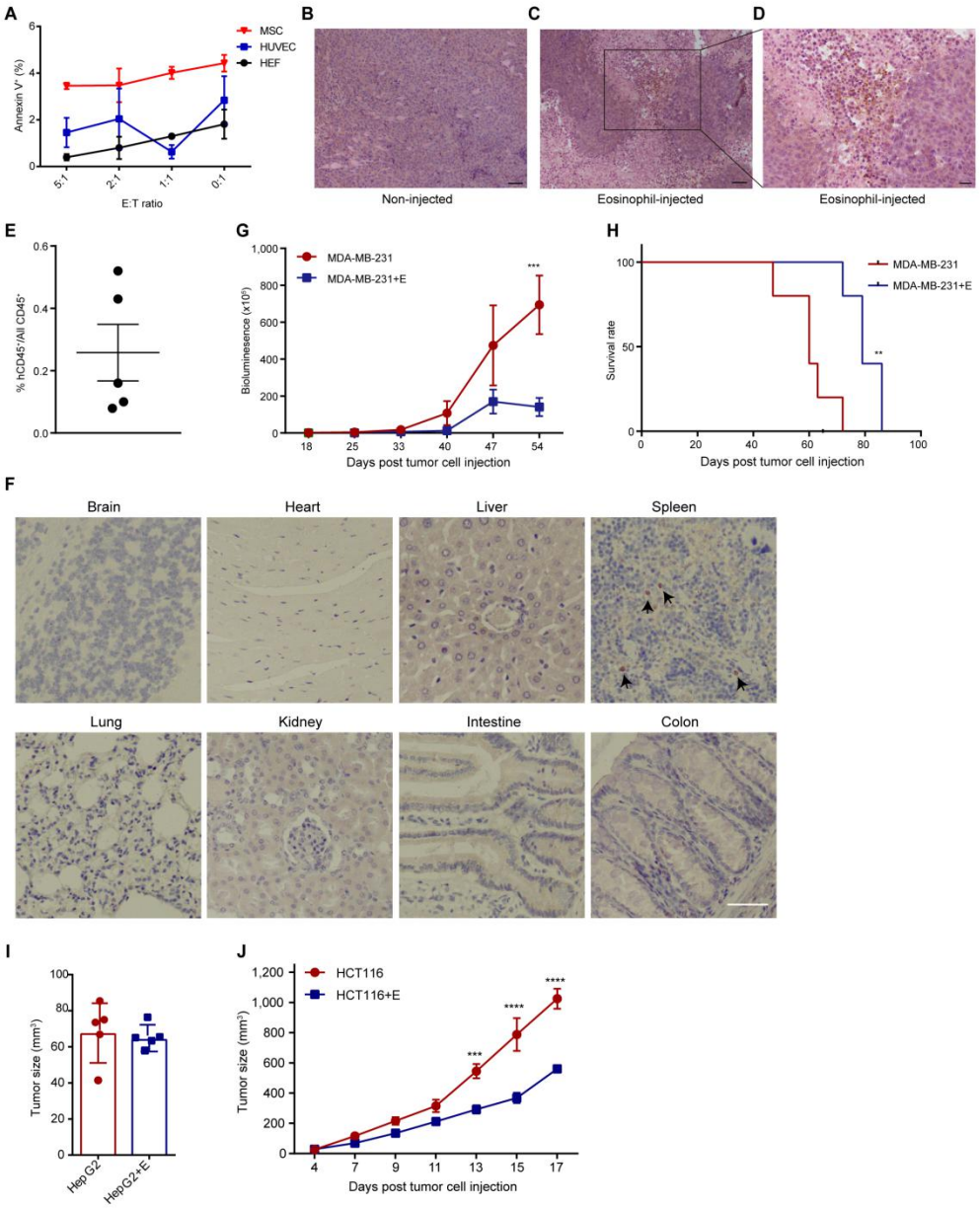

Figure S2. The infiltration of eosinophils into tumors and the anti-tumor activity of hESC-derived eosinophils, related to Figure 3, Figure 4.

(A) H1-derived eosinophils were cocultured with primary human umbilical vein endothelial cells (HUEVC), human embryonic fibroblasts (HEF) and human mesenchymal stroma cells (MSC) as target cells respectively. Annexin V^+ cells were shown as the mean percentage value ± SD (n=3), representative data from 3 independent experiments.

(B-D) Immunohistochemical analysis of H1-derived eosinophils infiltrated in HCT116 tumors, as detected by EPX antibody, in (B) control tumor, (C and D) H1-derived eosinophils injected tumor. For (B) and (C), scale bar, 50μm; for (D), scale bar, 20μm.

(E) Statistics showing the percentage of human $CD45^+$ cells in tumor tissues of MDA-MB-231

cell-burdened mice at 48 h after injection of H1-derived eosinophils (n = 5 mice); data shown as the mean values ± SEM.

(F) Immunohistochemical analysis of H1-derived eosinophils infiltrated in main organs, as detected by EPX antibody (arrowhead in the spleen indicate human EPX^+ eosinophils), scale bar, 50 μm.

(G) The MDA-MB-231 tumor cell burden of each group was measured on the indicated days after tumor cells injection by bioluminescent imaging (n = 5 mice for each group). Statistical significance was assessed using two-tailed ANOVA, where ***$p < 0.001$; data shown as the mean values ± SEM.

(H) Kaplan-Meier curve representing the survival rate of the experimental groups in the MDA-MB-231 xenograft mouse models (n = 5 mice for each group). Statistical analysis was calculated using log-rank (Mantel-Cox) test, where **$p < 0.01$.

(I) Tumor size of HepG2 on day 7 after tumor cell injection (n = 5 mice for each group), data shown as the mean values ± SD.

(J) HCT116 tumor size of each group determined on the indicated days after tumor cell injection (n = 5 mice for each group). Statistical significance was assessed using two-tailed ANOVA, where ***$p < 0.001$ and ****$p < 0.0001$; data shown as the mean values ± SEM.

Figure S3

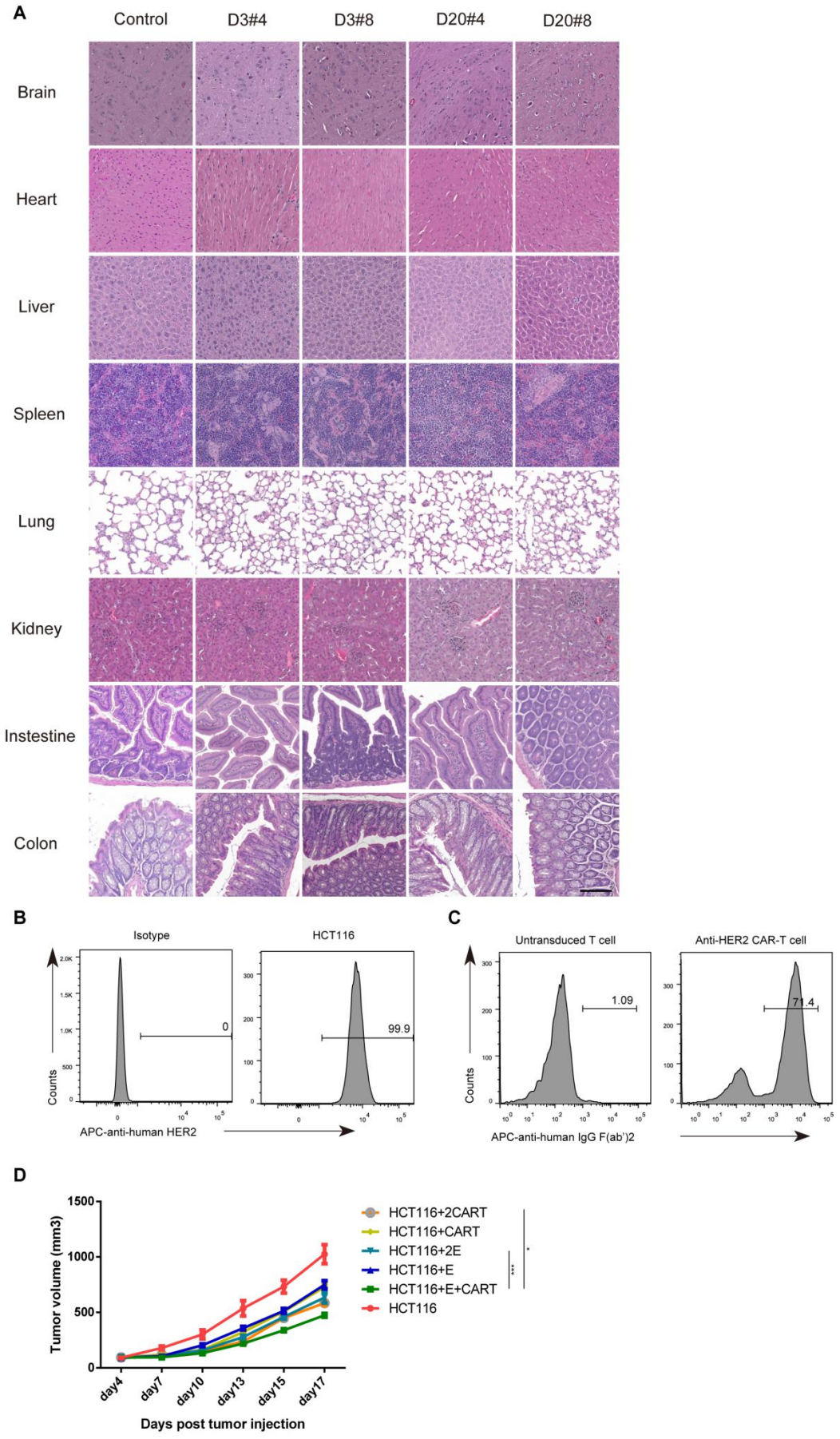
A
Control
D3#4
D3#8
D20#4
D20#8
Brain
Heart
Liver
Spleen
Lung
Kidney
Instestine
Colon
B
Isotype
HCT116
Counts
APC-anti-human HER2
0
99.9
C
Untransduced T cell
Anti-HER2 CAR-T cell
Counts
APC-anti-human IgG F(ab')2
1.09
71.4
D
Tumor volume (mm3)
Days post tumor injection
day4
day7
day10
day13
day15
day17
HCT116+2CART
HCT116+CART
HCT116+2E
HCT116+E
HCT116+E+CART
HCT116
***
*

Figure S3. Histological analysis of major organs of mice injected with H1-derived eosinophils and the generation of CAR-HER2 T cells, related to Figure 4.

(A) Sections of brain, heart, liver, spleen, lung, kidney, intestine and colon were collected after the injection of H1-derived eosinophils at 4 × 10^6 cells and 8 × 10^6 cells per mouse at day 3 and day 20 respectively and stained with Hematoxylin and Eosin for the detection of changes in tissue morphology (D3#4: day 3, 4 × 10^6 cells; D3#8, day 3, 8 × 10^6 cells; D20#4, day 20, 4 × 10^6 cells; D20#8: day 20, 8 × 10^6 cells), scale bar, 100 μm.

(B) Representative flow histogram showing HER2 expression of HCT116 cells.

(C) Representative flow histogram showing anti-HER2 CAR expression of T cells.

(D) HCT116 tumor size of each group measured on the indicated days after tumor cell injection (n=5 mice for each group). Statistical significance was assessed using two-tailed ANOVA, where *$p < 0.05$, and ***$p < 0.001$; data are shown as the mean values ± SEM.

Figure S4

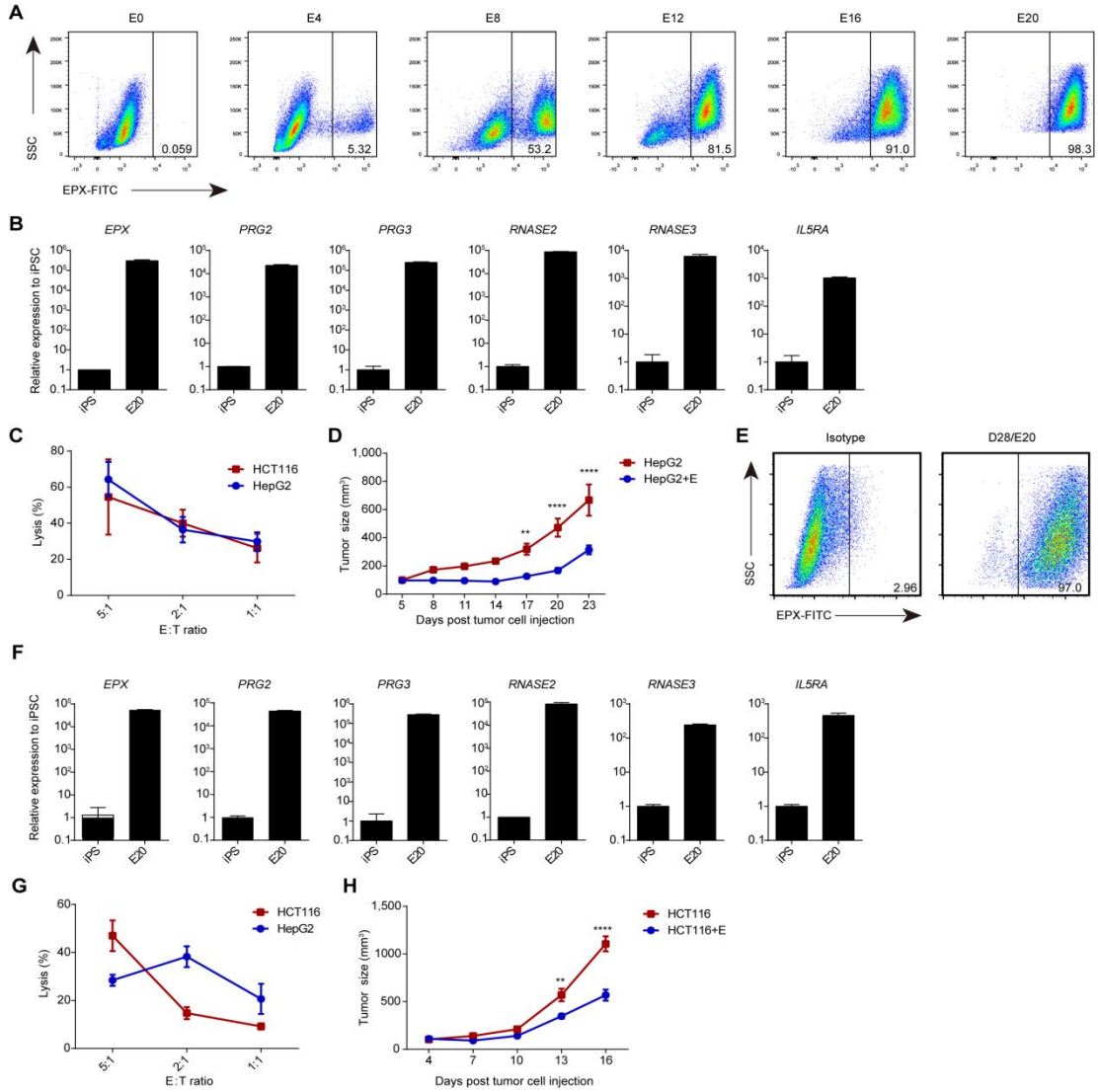

Figure S4. Efficient generation of eosinophils from human iPSCs.

(A) Representative flow plots from 3 independent experiments showing the kinetics of EPX$^+$ cell numbers during eosinophil differentiation from iPS-#7 cells.

(B) qPCR analysis of key gene expression in iPS-#7 cells and iPS-#7-derived eosinophils recovered on E20 (n = 3). Data shown as the mean percentage value ± SD. This is a representative data from 3 independent experiments.

(C) Cytotoxicity of the iPS-#7-derived eosinophils toward HCT116 and HepG2 target cells at the indicated effector-to-target ratios, respectively (n = 3). The lysis rate of target cells was shown as the mean percentage value ± SD. This is a representative data from 3 independent experiments.

(D) Tumor size determined on the indicated days after HepG2 tumor cells injection (n = 5 mice for each group). Statistical significance was assessed using two-tailed ANOVA, where **p < 0.01 and ****p < 0.0001; data shown as the mean values ± SEM.

(E) Representative flow plots from 3 independent experiments showing EPX$^+$ E20 eosinophil differentiation from iPS-#8 cells.

(F) qPCR analysis of key gene expression in iPS-#8 cells and iPS-#8-derived eosinophils

recovered on E20 (n = 3). Data shown as the mean percentage value ± SD. This is a representative data from 3 independent experiments.

(G) Cytotoxicity of the iPS-#8-derived eosinophils toward HCT116 and HepG2 target cells at the indicated effector-to-target ratios, respectively (n = 3). The lysis rate of target cells was shown as the mean percentage value ± SD. This is a representative data from 3 independent experiments.

(H) Tumor size determined on the indicated days after HCT116 tumor cells injection (n = 5 mice for each group). Statistical significance was assessed using two-tailed ANOVA, where **$p < 0.01$ and ****$p < 0.0001$; data shown as the mean values ± SEM.

SUPPLEMENTAL TABLES

Table S1. List for qPCR primers, related to Figure 2, Figure S4 .

*β-Actin*_ Forward	GACAGCAGTCGGTTGGAGCG
*β-Actin*_ Reverse	GGGACTTCCTGTAACAACGCATC
*EPX*_ Forward	GTCCTGCGAGACTGCATAGC
*EPX*_ Reverse	TATAATCTGCGGCCCGAACAA
*PRG2*_ Forward	AAACTCCCCTTACTTCTGGCT
*PRG2*_ Reverse	GCAGCGTCTTAGCACCCAA
*PRG3*_ Forward	TCTGGAGAGCCTAGAGACACA
*PRG3*_ Reverse	CCTCCGTCAGAGCCAAGTC
*RNASE2*_ Forward	TTTACCTGGGCTCAATGGTTTG
*RNASE2*_ Reverse	TGCATCGCCGTTGATAATTGT
*RNASE3*_ Forward	CCCACAGTTTACGAGGGCTC
*RNASE3*_ Reverse	ACCCGGAATCTACTCCGATGA
*IL5RA*_ Forward	ATCATCGTGGCGCATGTATTAC
*IL5RA*_ Reverse	AAAGAACTTGAGCCAAACCAGT

SUPPLEMENTAL EXPERIMENTAL PROCEDURES

Mice

Mouse experiments were conducted according to the protocol approved by the Institutional Animal Care and Use Committee (IACUC) of Peking University. All of the mice were NOD-Prkdc^{scid} Il2rgtm1/Vst (NPG) mice (Stock Number: VS-AM-001) purchased from Beijing Vitalstar Biotechnology, and they ranged from 8 to 12 weeks of age.

Cord blood

This study was approved by the Institute of Review Board in Peking University (IRB 00001052-15087) and conducted according to the approved protocol. Samples were collected from consenting donors according to ethically approved procedures at China-Japanese Friendship Hospital and 307 Hospital of People's Liberation Army of China.

Cell culture

Human embryonic stem cells (H1) were obtained from Wicell (NIH: hESC-10-0043), and their usage was annually approved. H1 cells were cultured in Matrigel (BD Biosciences, Cat: 354230)-coated plates with pluripotent stem cell culture medium (PSCM, PSCeasy, Beijing CELLAPY Biotechnology) under 20% O_2 and 5% CO_2 at 37 °C. H1 cells were passaged by treatment with 0.5 μM EDTA (Gibco, Cat: 25300-062) for 5-6 min at 37 °C, and cells were collected and split at 1 to 6 - 1 to 10 ratios with pluripotent stem cell culture medium containing 5 μM Y-27632 (Selleck, Cat# S1049).

iPS cells (iPS-#7, iPS-#8) were purchased from Cauliscell Biotechnology and were cultured in Matrigel-coated plates with pluripotent stem cell culture medium (PSCeasy, Beijing CELLAPY Biotechnology). iPS cells were passaged by splitting at ratios of nearly 1 to 6 following treatment with 0.5 μM EDTA for 5-6 min at 37 °C, and then the cells were collected and plated with pluripotent stem cell culture medium containing 5 μM Y-27632.

HCT116 and MDA-MB-231 cell lines were obtained from the National Infrastructure of Cell Line Resource (Beijing, China). The HepG2 cell line was a gift from Kuanhui Xiang (Peking University Health Science Center). All these cell lines were transduced with lentiviral GFP-luc vector, were sorted to isolate GFP$^+$ populations, and then were cultured in DMEM (Thermo Fisher Scientific) plus 10% FBS (HyClone), 1% GlutaMAX (Gibco), 1% PS (Gibco) and 1% NEAA (Gibco) under 5% CO_2 at 37 °C conditions. Trypsin-EDTA (0.25%) was used for passage.

Human embryonic fibroblasts (HEFs) were isolated and approved by IRB of Clinical Research Ethics Committee of China-Japan Friendship Hospital (Ethical approval No: 2009–50) and Stem Cell Research Oversight of Peking University (SCRO201103-03). They were cultured in DMEM (Thermo Fisher Scientific) plus 10% FBS (HyClone), 1% GlutaMAX (Gibco), 1% PS (Gibco) and 1% NEAA (Gibco) under 5% CO2 at 37 ℃ conditions. Human umbilical vascular and endothelial cells (HUVECs) were purchased from Lonza and cultured according to the manufacturer’s manual. Trypsin-EDTA (0.25%) was used for the passage of HEFs and HUVECs.

Eosinophil differentiation from human ESCs and iPSCs

Pluripotent stem cells were cultured in Matrigel-coated plate with low density from 1 × 10^4~5 × 10^4/well in 6-well plate in pluripotent stem cell culture medium at day 1 before the differentiation. At differentiation day 0, Activin A (20ng/ml), BMP4 (20ng/ml) (StemImmune LLC, Cat: HST-B4-0100) and CHIR-99021 (3-5 μM) were administrated in the medium RPMI 1640 supplemented with B27 (without vitamin A) and 50 μg/ml ascorbic acid. From day 2 to day 6, 5 ng/ml BMP4, 50 ng/ml human vascular endothelial growth factor (VEGF, StemImmune LLC, Cat: HVG-VF5-1000), 50 ng/ml human basic fibroblast growth factor (bFGF, Origene, Cat: TP750002) and 10 μM SB-431542 (Selleck, Cat: S1067) were added. From day 6 to day 12, 5 ng/ml BMP4, 10 ng/ml VEGF, 20 ng/ml recombinant human stem cell factor (SCF, StemImmune LLC, Cat: HHM-SF-1000), 30 μM NAC (Sigma, Cat: A7250-5G), and 2 μM minocycline hydrochloride (Selleck, Cat: 3268) were supplemented in IMDM (Thermo Fisher Scientific) containing B27 without vitamin A and 50 μg/ml ascorbic acid. After day 12, eosinophil induction medium was used, which consisted of IMDM supplemented with B27 (without vitamin A), 30 μM NAC, 2 μM minocycline hydrochloride, 10 ng/ml human recombinant interleukin-3 (IL3, StemImmune LLC, Cat: HCT-I3-1000) and 10 ng/ml human recombinant interleukin-5 (IL5, Novoprotein, Cat: CI59).

Isolation of human primary naïve eosinophils from cord blood

Human primary naïve eosinophils were isolated based on anti-CD16-negative selection protocol via certain modifications (Wacht et al., 2018). Briefly, cord blood unit was diluted by sterile PBS, aliquoted gently to human lymphocyte separation medium (DRKEWE, Cat: DKW-KLSH-0100), and centrifuged at 1,500 rpm for 20 min according to the manufacturer' s protocol to obtain blood cells separated in different layers. Cell pellets in the bottom layer, which contained mainly granulocytes and red blood cells, were collected and suspended in 1 × RBC lysis buffer (Biolegend, Cat: 420301) to lyse the red blood cells according to the product manual. After lysis of red blood cells, the remaining cells were mainly granulocytes. They were washed twice with PBS, centrifuged at 1,500 rpm for 5 min. Cell pellets were then collected and stained with BV421 anti-human CD45 (Biolegend, Cat: 304032) and PE-Cy7 anti-human CD16 (Biolegend, Cat: 302016). Then the $CD45^+CD16^-$ cell population were isolated by the flow cytometer (MoFlo XDP) and collected in sterile PBS. These $CD45^+CD16^-$ cells were regarded as primary naïve eosinophils.

Isolation of human mesenchymal stem cells from cord blood

For mesenchymal stromal cells, monocyte cells after lymphocyte separation were cultured in DMEM (Gibco) containing 10% FBS (Hyclone) for 48 hours and the suspending cells were discarded. Adherent mesenchymal stromal cells were further cultured to 80% confluence.

Flow cytometry analysis

For surface marker detection, cultured cells were collected at the indicated times, digested with accutase (Millipore, Cat: SCR005) at 37 °C for 5 min, diluted with an equal volume of PBS (Corning, Cat: 21-040-CV), centrifuged at 1,800 rpm for 3 min to obtain cell pellets, and resuspended with PBS containing 0.5% BSA (Sigma, Cat: A1470–100G) to form a single-cell suspension. Next, the indicated antibodies were added, and they were incubated with the cells

for 15 min in the dark at room temperature. Then, the cells were washed three times with PBS, were suspended in 300 μl of PBS, and then were filtered through a 40 μm nylon cell strainer for analysis. Each antibody (0.2 μl) was added to each sample. The antibodies used were as follows: 7-AAD (BD Pharmingen, 559925), BV421 anti-human CD45 (Biolegend, Cat: 304032), PE anti-human CD69 (Biolegend, Cat: 310906), PE anti-human CD11b (Biolegend, Cat: 301306), PE-Cy7 anti-human Siglec-8 (Biolegend, Cat: 347112), and APC-Cy7 anti-human CD34 (Biolegend, Cat: 343614), and the Isotype Ctrl Antibody are: Brilliant Violet 421™ Mouse IgG1, κ Isotype Ctrl Antibody (Biolegend, Cat: 400157), PE/Cyanine7 Mouse IgG1, κ Isotype Ctrl Antibody (Biolegend, Cat: 400125), PE Mouse IgG1, κ Isotype Ctrl Antibody (Biolegend, Cat: 400111), APC/Cyanine7 Mouse IgG2a, κ Isotype Ctrl Antibody (Biolegend, Cat: 400229).

For intracellular staining of EPX, the cultured cells were collected at the indicated times and were digested into single-cell suspensions as described above. Then they were stained with Fixable Viability Stain 575V (BD Horizon™, Cat: 565694) according to the product manual. Next, the cells were fixed and permeabilized using a BD Cytofix/Cytoperm™ Fixation/Permeabilization kit (BD, Cat: 554714), and then they were stained with an anti-EPX antibody (Abcam, Cat: ab190715) according to the manual; a proportion of the cells were stained with mouse clonal IgG1 (BD Pharmingen™, Cat: 555751) as an isotype control. The cells were then washed twice with 1 × BD Perm/Wash buffer before being incubated with Alexa Fluor 488-AffiniPure donkey anti-mouse IgG (1:200 dilution, Jackson ImmunoResearch, Cat: 715-545-150) at 37 °C for 15 min. Then, the cells were washed twice and were filtered through 40 μm nylon cell strainer for analysis.

To analyze the infiltration of human ESC-derived eosinophils in solid tumors, mice were euthanized, and tumors were isolated. Isolated tumors were cut into 1 mm pieces with scissors and then were digested by incubation with 1 ug/ml Collagenase IV (Sigma, Cat: 17104019) and 1mg/ml Dnase (Sigma, Cat: DN25-1G) at 37 °C and 5% CO_2 for 30 min. Single cells were pipetted to a tube after digestion and were collected by centrifugation at 1800 rpm for 5 min. Tumor-derived cells were stained with PE anti-mouse CD45 (Biolegend, Cat: 103106) and BV421 anti-human CD45 (Biolegend, Cat: 328114) antibodies, were washed three times with PBS, and were filtered through a 40 μm nylon cell strainer for flow cytometry.

Flow cytometry analysis was conducted using LSRFortessa (BD). The data were analyzed using FlowJo-V10 (BD).

Giemsa staining

Differentiated cells were collected, counted and then centrifuged at 1,800 rpm for 3 min. Cell pellets were resuspended in PBS at a density of 5 × 10^6/ml, and 20- 30 μl of cells were added to adhesive microscope slides (CITOTEST, Jiangsu, Cat: 188105) and were centrifuged in StatSpin CytoFuge 2 (CYTOCENTRIFMGE) according to the protocol. Cells on the slides were fixed by incubation with 100% methanol (Beijing Chemical Work) in a glass bottle for 5 min. After air-drying, cells were stained by adding 200 μl of Eosinophil-specific staining solution A (Carbol 2R) (Baso Zhuhai, Cat: DA0164) for 5 minutes, which was followed by ten times of distilled water wash. Then, 200 ul of Eosinophil-specific staining solution B (Baso

Zhuhai, Cat: DA0164) were added and treated for 5 minutes. The solutions were discarded, and the slides were washed 4-5 times with distilled water. Stained cells were observed under a microscope (Olympus, BX-43), and pictures were taken with Cellsens software (Olympus Life Science).

Electron microscopy

Eosinophils differentiated on day 28 (D28/E16) were fixed with 2% paraformaldehyde / 2.5% glutaraldehyde in 0.1 M phosphate buffer, pH 7.4, for 5 min at 37 ℃, and then they were incubated for another 30 min at room temperature and overnight at 4 ℃. After rinsing several times in phosphate buffer, cells were postfixed in 2% OsO_4 with 1.5% potassium ferrocyanide for 2 h at room temperature. Following several washes in distilled water, samples were stained with 2% aqueous uranyl acetate overnight at 4 °C. After washing several times in distilled water, the cultures were dehydrated in a graded alcohol series and subsequently were embedded in Spurr's resin (SPI supplies, PA, USA). Ultrathin sections (70 nm) were cut with a diamond knife on an ultramicrotome (UC7, Leica Microsystem) and were collected on copper grids with a single slot. Sections were stained with uranyl acetate and lead citrate and then were observed under an electron microscope (Tecnai G2 Spirit, FEI) at 120 kV.

Immunofluorescence

The cells were fixed in 4% paraformaldehyde (DingGuo, AR-0211) at room temperature for 15 min and blocked with PBS that contained 0.2% Triton X-100 (Sigma-Aldrich, T8787) and 3% normal donkey serum (Jackson Immuno Research, 017-000-121) at room temperature for 45 min. The cells were incubated with primary antibodies at 4°C overnight. Secondary antibodies (Jackson ImmunoResearch) were incubated at room temperature for 1 hr. The nuclei were stained with DAPI (Roche Life Science, 10236276001). Antibody details were provided below.
anti-EPX (1:200, Abcam, Cat: ab190715); anti-Bsp-1 (1:200, BD Pharmingen, Cat: 552754); anti-MBP1 (1:200, invitrogen, Cat: PA5-112670); anti-RceR1 alpha (1:200, eBioscience, Cat: 11589942); anti-CD203c (1:200, biolegend, Cat: 324610); anti-EDN (1:200, CUSABIO, Cat: P10153); anti-ECP (1:200, CUSABIO, Cat: P12724).

RNA sequencing and bioinformatics analysis

During H1 differentiation, total RNA was isolated from cultured cells on day 0 (H1), day 12 (E0), day 16 (E4), day 20 (E8), day 24 (E12), day 28 (E16), and day 32 (E20) using RNeasy Plus Micro kit (Qiagen, 74034). Total RNA of cord blood primary naïve eosinophils was isolated using the same kit. RNA sequencing libraries were constructed using an NEB Next, Ultra RNA Library Prep kit for Illumina (NEB England BioLabs, E7530L). The fragmented paired-end libraries were sequenced using an Illumina HiSeq-PE150. All sequencing was performed at Novogene.

For bioinformatics analysis of the RNA-seq data, Fastq reads were aligned to the human reference genome (hg19) or mouse reference genome (mm10) using TopHat. Counting and FPKM values were calculated with cuffquant and cuffnorm, respectively. Clustering analysis and gene expression heatmaps in Figures were based on FPKM values. DESeq2 was used with default parameters to identify differentially expressed genes between samples. We used

log2 (fold change) >1 or < -1 and FDR < 0.01 as the cutoff.

Quantitative real-time PCR

Total RNA was isolated from the indicated cells with an RNA isolation kit (QIAGEN, Cat: 74034) according to the manufacturer's protocol. The Easy transcriptase kit (Transgene, Cat: AT311–03) was used for synthesizing cDNA from total RNA. Quantitative real-time PCR was performed in triplicate from at least three biological samples with a BIO-RAD CFX Connect™ Real-Time PCR Detection System (Bio-Rad, Cat: 1855201). Quantitative PCR was carried out in a volume of 20 μl using FastStart Essential DNA Green Master (Roche, Cat: 06924204001). The PCR protocol was as follows: first, 95 °C for 10 min to activate the polymerase, followed by 40 cycles at 95 °C for 10 s (for denaturation), 60 °C for 10 s (for annealing), and 72 °C for 10 s (for extension). Values for mRNA expression were normalized to the expression of H1 or iPSC. The primer sets used to detect single genes are listed in Table S1.

Lentiviral vectors and transduction

The lentiviral vector (Plenti3) EF1a-GFP-2A-Luc2-SV40-puro (GFP-luc for short), which encodes separate GFP protein and luciferase, was packaged, and the titre was determined according to the protocol previously described (Xiao et al., 2019). HCT116, MDA-MB-231 and HepG2 cell lines were transduced with the lentiviral vectors with 8 μg/ml polybrene (Yeasen, Cat: 40804ES86), and then the GFP^+ cells were flow sorted and propagated, and the luciferase activity of each was confirmed before further use.

Isolation, activation and infection of human T cells

All Peripheral Blood Mononuclear Cells (PBMCs) used in our study were obtained from healthy donors who provided informed consent (Blood Center of Beijing Red Cross Society). Human T lymphocytes were cultured in RMPI-1640 medium (Gibco, USA) supplemented with 10% FBS and 300 U/ml interleukin-2 (Peprotech, USA). After 48 hours of activation with anti-human CD3/CD28 Dynabeads (Gibco, USA), 8 μg/ml polybrene (Millipore, USA) and 300 U/ml IL-2 were added to each well and T cells were transduced twice over the next 48 h with meso-CAR lentivirus by spinoculation for 1 h. Transduction efficiency was determined by flow cytometry 7 days later.

Immunohistochemistry and histological analysis

To analyze the infiltration of human ESC-derived eosinophils in solid tumors and mouse main organs, tumor tissues and mouse main organs were fixed with formalin (10% and 20% respectively 24 h) at room temperature. After paraffinization, 5 μm slices were cut and affixed on slides for immunohistochemical staining. We used the anti-EPX antibody (Abcam, Cat: ab19075) to identify eosinophils according to the manual (ZSGB-BIO, SP-9000). Main organs of mouse were collected after the injection of hPSC-derived eosinophils at 4 × 106 and 8 × 106 per mouse at day 3 and day 20 respectively, Hematoxylin and Eosin(H&E) staining was used for tissue and cell identification.

***In vitro* cytotoxicity assays**

Tumor cells bearing the GFP-luc transgene were seeded at a density of 1 × 10^4cells/well in

96-well plates in 100 ul DMEM containing 10% FBS. Six to ten hours later, the eosinophils were added to the target cells at E (effector): T (target) = 5: 1, 2: 1, 1: 1, and 0: 1, and the medium volume of eosinophil suspension was 100 μl per well. After incubation for 20 h, the apoptotic cells of the tumor target cells were quantified by a standard bioluminescence assay based on luciferase using a multimode plate reader (PerkinElmer). The percentage of lysed cells was calculated using the following equation: % lysis = 100 × (spontaneous death RLU - test RLU) / (spontaneous death RLU). RLU: relative light units.

***In vivo* tumor assay**

For forming inoculated tumors, luciferase-marked target cells were injected subcutaneously into the recipient NPG mice at a dose of 5×10^4 cells per mouse, which was followed by two intravenous injections of eosinophils; each mouse received 2×10^6 eosinophils suspended in 100 μl of culture medium on day 3 and day 6. The control groups were injected with only an equal volume of culture medium to enable comparison with the experimental groups. The tumor burden of each mouse was monitored by *in vivo* bioluminescence imaging using Xenogen IVIS (Caliper Life Sciences). Mice were injected intraperitoneally with 150 mg/kg D-luciferin (GoldBio, Cat: LUCK-100) and were imaged 10 min later;

For forming established tumors, 1.5×10^6 HepG2 tumor cell were injected subcutaneously and 2×10^6 eosinophils (pre-activated 20 hour with 10 ng/ml IFNγ and 10 ng/ml TNFα) were intravenously injected on day 7 and day 10; 1×10^6 A375 tumor cell were injected subcutaneously and 2×10^6 eosinophils (pre-activated 20 h with 10 ng/ml IFNγ and 10 ng/ml TNFα) were intravenously injected on day 6 and day 9; 1×10^6 HCT116 tumor cell were injected subcutaneously and 2×10^6 eosinophils (pre-activated 20 h with 10 ng/ml IFNγ and 10 ng/ml TNFα) were intravenously injected on day 4 and day 7;

For evaluating the combination effects of CAR-T and hESC-derived eosinophils, we designed CAR-T or hESC-derived eosinophils alone as controls. Tumor cells were injected subcutaneously at a dosage of 1×10^6 HCT116 tumor cells per mouse. Two intravenous injections of eosinophils, CAR-T cells or their combination were performed. Each mouse received 2×10^6 eosinophils, which were pre-activated 20 h with 10 ng/ml IFNγ and 10 ng/ml TNFα on day 4 and day 7. In the following day, 1×10^6 CAR-T cells were respectively injected. To increase the dose of CAR-T or hESC-derived eosinophils, each mouse received 4×10^6 eosinophils on day 4 and day 7, or each mouse received 2×10^6 CAR-T. The control groups were injected with only an equal volume of culture medium to enable comparison with the experimental groups. The tumor size was measured at the indicated time points using the following formula: V = 1/2 × (length × width × width). Tumor-bearing mice in this study were randomized to different groups. Mice with large tumor masses more than 15 mm in length were euthanized.

SUPPLEMENTAL REFERENCES

Wacht, G., Poirot, A., Charles, A.L., Radosavljevic, M., Uring-Lambert, B., de Blay, F., Geny, B., Bahram, S., and Barnig, C. (2018). FACS - based isolation of human eosinophils allows

purification of high quality RNA. J Immunol Methods *463*, 47-53.
Xiao, X., Lai, W., Xie, H., Liu, Y., Guo, W., Liu, Y., Li, Y., Li, Y., Zhang, J., Chen, W*., et al.* (2019). Targeting JNK pathway promotes human hematopoietic stem cell expansion. Cell discovery *5*, 2.